Supporting Information

Reactivity of diphosphinodithio ligated nickel(0) complex toward alkyl halides and resultant nickel(I) and nickel(II)-alkyl complexes

*Ailing Zhang, Congxiao Wang, Xiaoyu Lai, Xiaofang Zhai, MaoFu Pang, Chen-Ho Tung and Wenguang Wang**

Key Lab for Colloid and Interface Chemistry of Education Ministry, School of Chemistry and Chemical Engineering, Shandong University, Jinan, 250100, China

Table of Contents

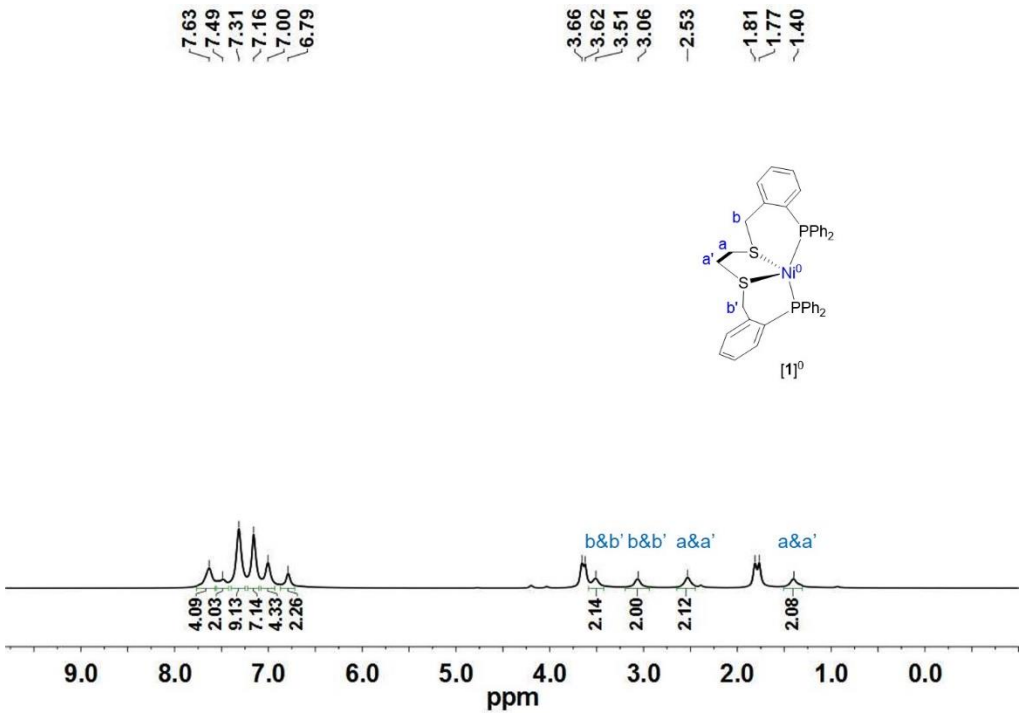

Fig. S1 ^{1}H NMR spectrum of [**1**]^{0} in THF-d_8.

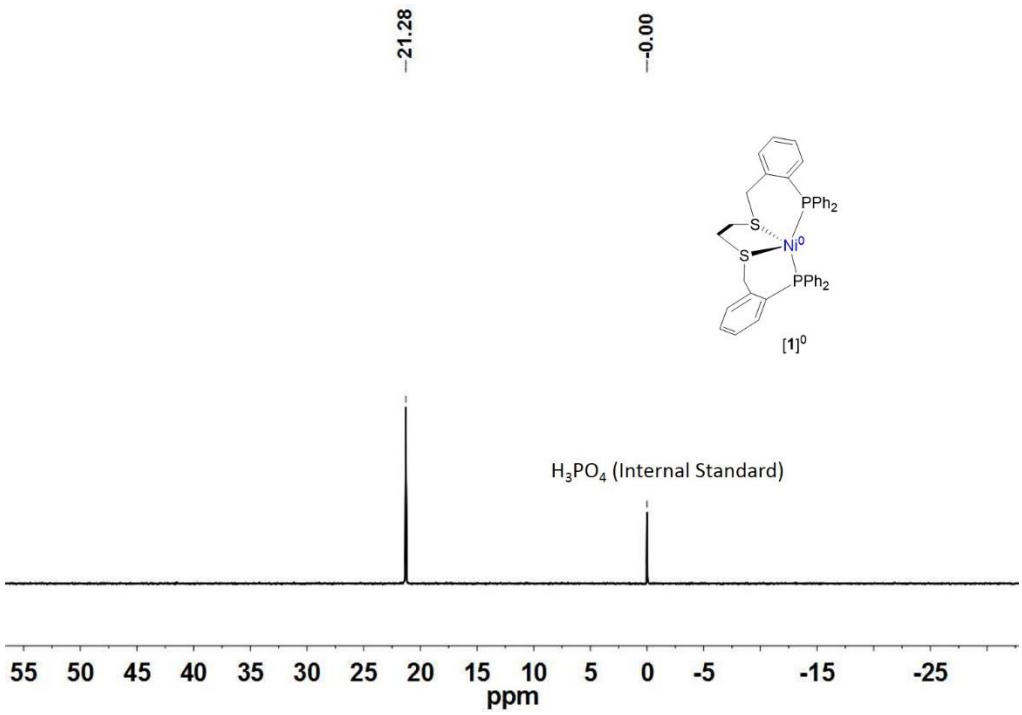

Fig. S2 ^{31}P NMR spectrum of [**1**]^0 in THF (H_3PO_4 as internal standard).

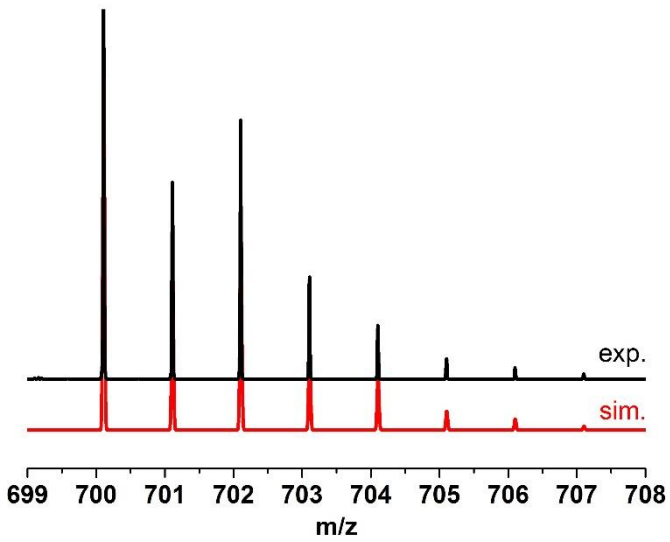

Fig. S3 ESI-MS spectrum of [**1**]^0 in toluene.

Results:

Calcd for [**1**]^0, 700.1087; found, 700.1071.

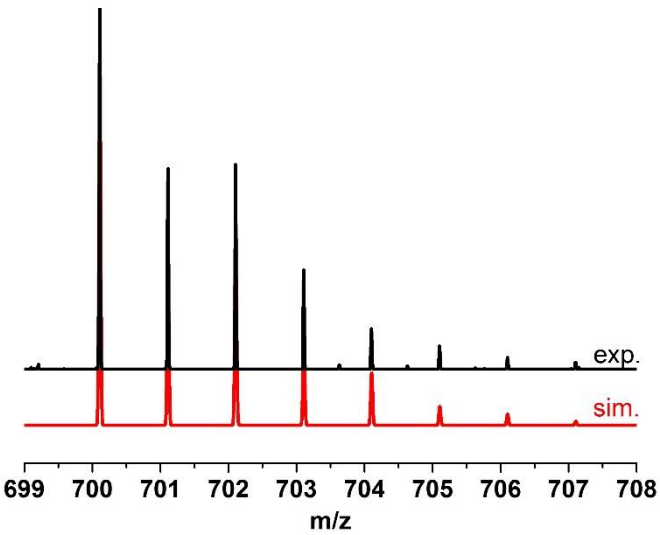

Fig. S4 ESI-MS spectrum of [**1**]BPh_4 in CH_2Cl_2.

Results:

Calcd for [**1**]BPh_4 , 700.1087; found, 700.1068.

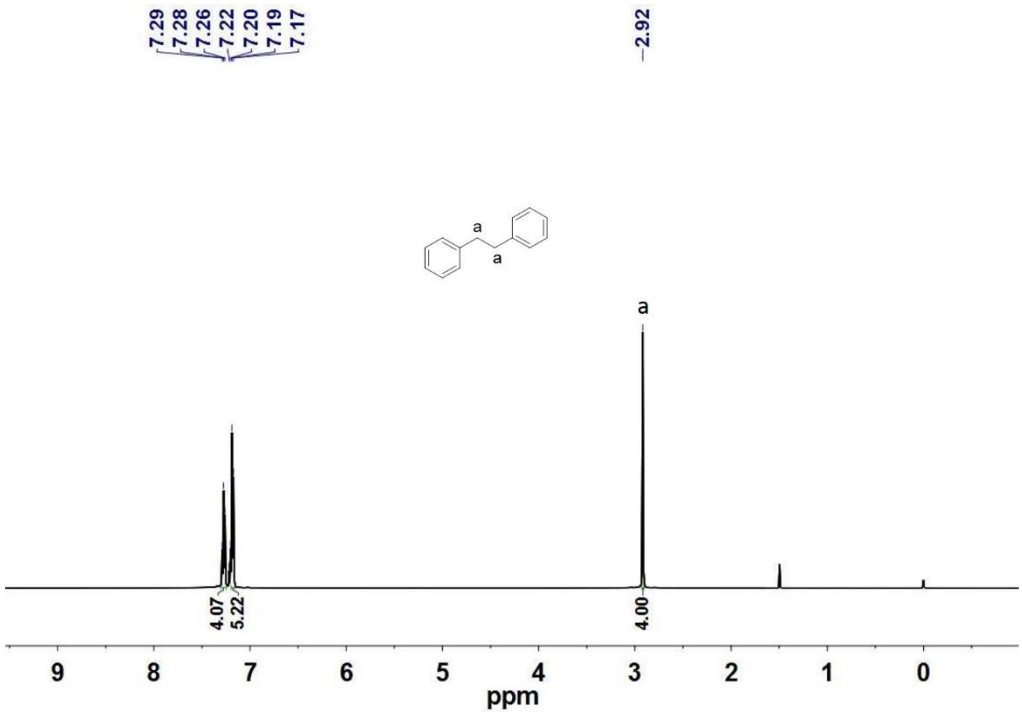

Fig. S5 ^{1}H NMR spectrum of 1,2-diphenylethane in $CDCl_3$.

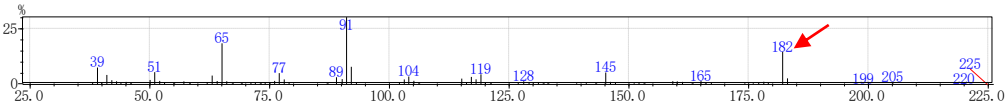

Fig. S6 GC-MS for the reaction mixture of [**1**]^0 with BnBr.

Results: Calcd for bibenzyl, 182.1096; found, 182.

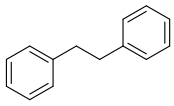

Chemical Formula: $C_{14}H_{14}$
Exact Mass: 182.1096
Molecular Weight: 182.2660
m/z: 182.1096 (100.0%), 183.1129 (15.1%), 184.1163 (1.1%)

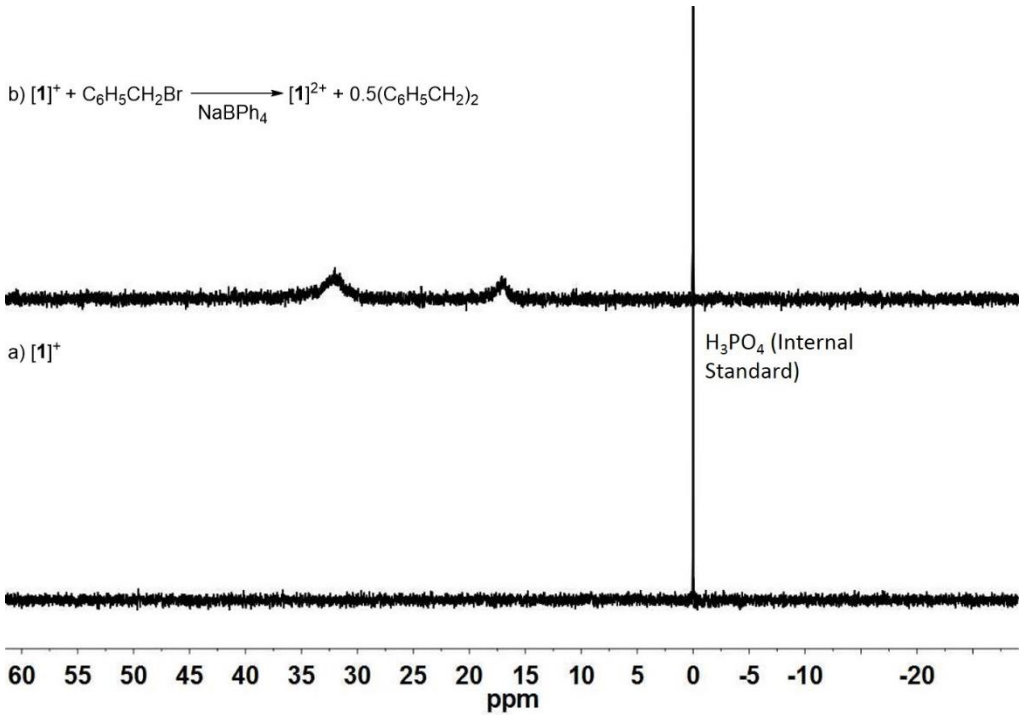

Fig. S7 ^{31}P NMR spectra for (a) [**1**]$^{+}$ in CH_2Cl_2 (H_3PO_4 as internal standard). (b) the reaction of [**1**]$^{+}$ with benzyl bromide, followed by treatment with $NaBPh_4$, the phosphorus spectrum is consistent with [**1**]$^{2+}$.

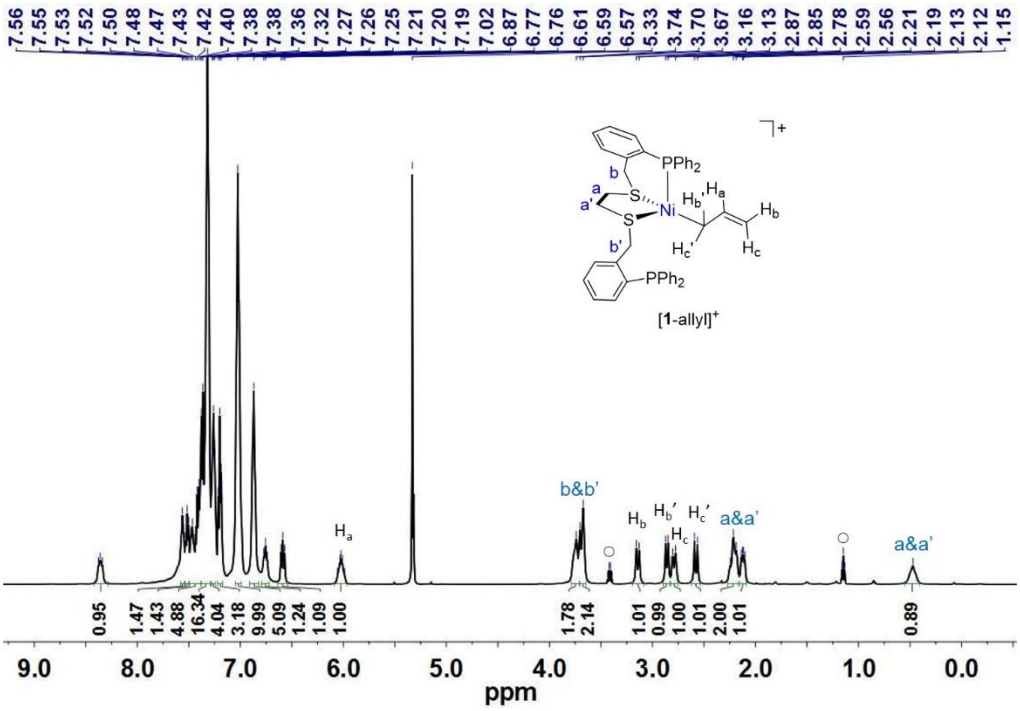

Fig. S8 ^{1}H NMR spectrum (500 MHz, CD_2Cl_2, 213K) of [**1**−allyl]BPh_4(○ = diethyl ether).

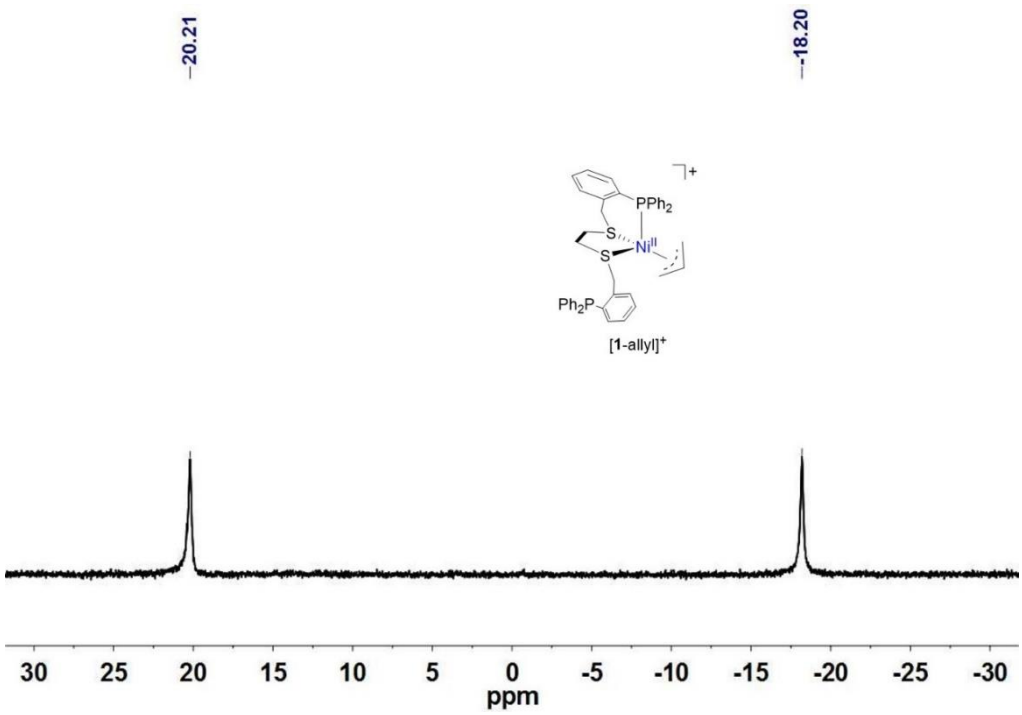

Fig. S9 ^{31}P NMR spectrum of [**1**−allyl]BPh_4 in CD_2Cl_2.

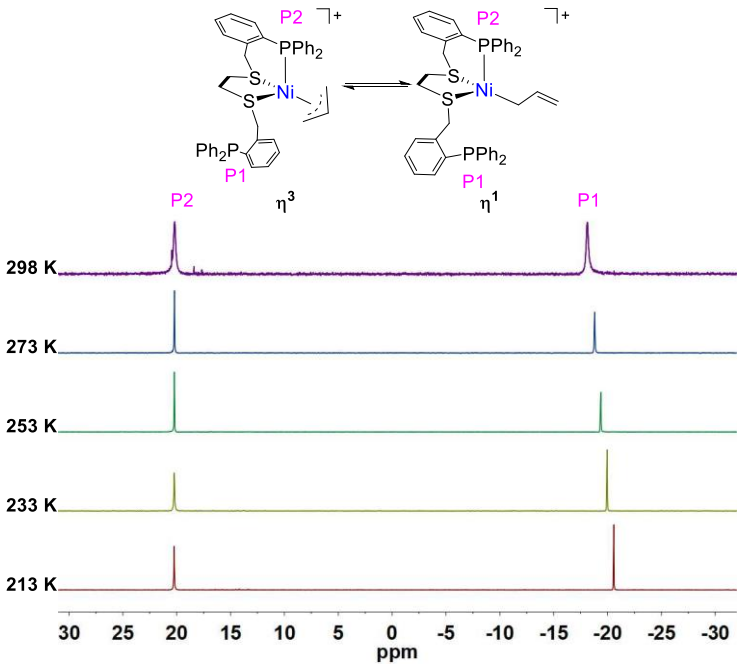

Fig. S10 VT ^{31}P NMR spectra (202 MHz, CD_2Cl_2) of [**1**−allyl]BPh_4.

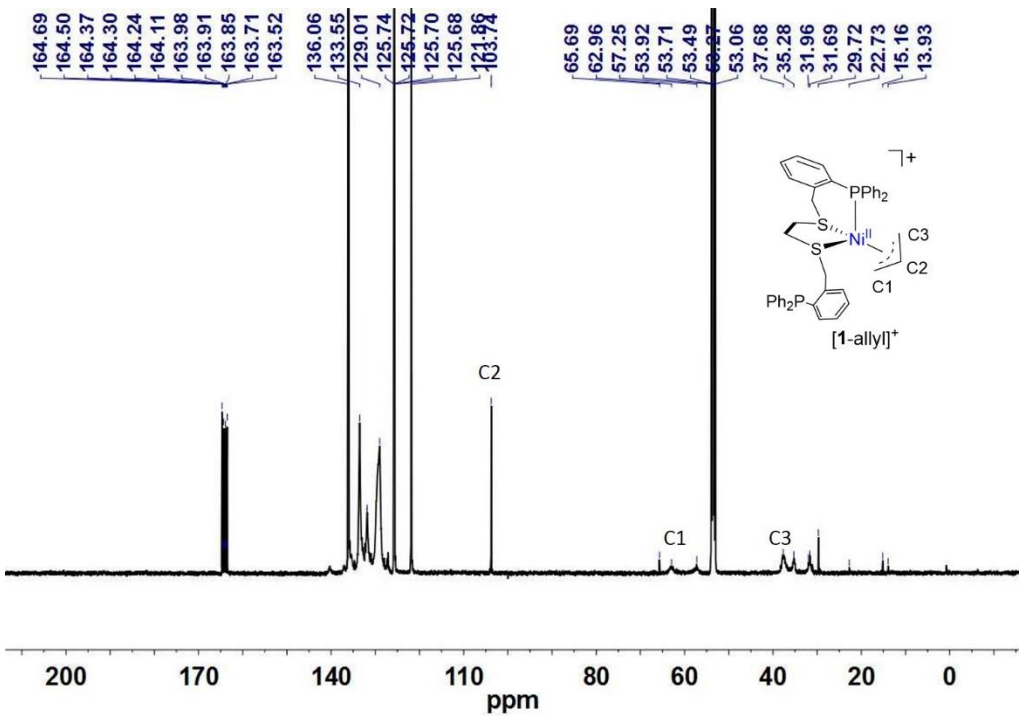

Fig. S11 ^{13}C NMR spectrum (126 MHz, CD_2Cl_2) of [**1**−allyl]BPh_4.

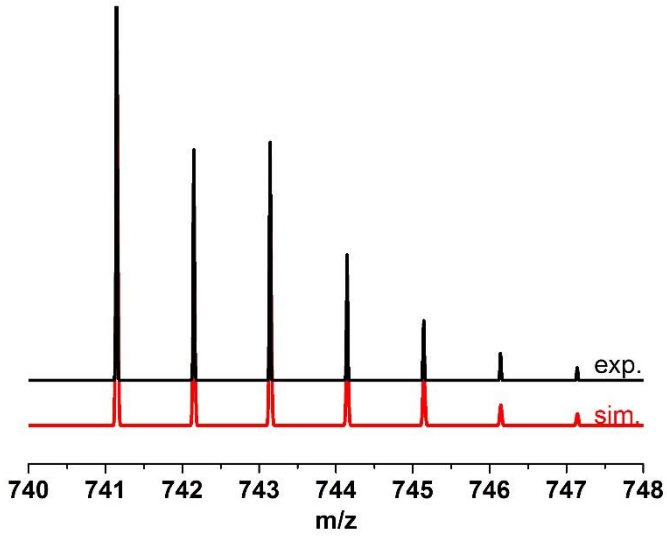

Fig. S12 ESI-MS spectrum of [**1**−allyl]BPh_4 in CH_2Cl_2.

Results:

Calcd for [**1**−allyl]BPh_4, 741.1478; found, 741.1458.

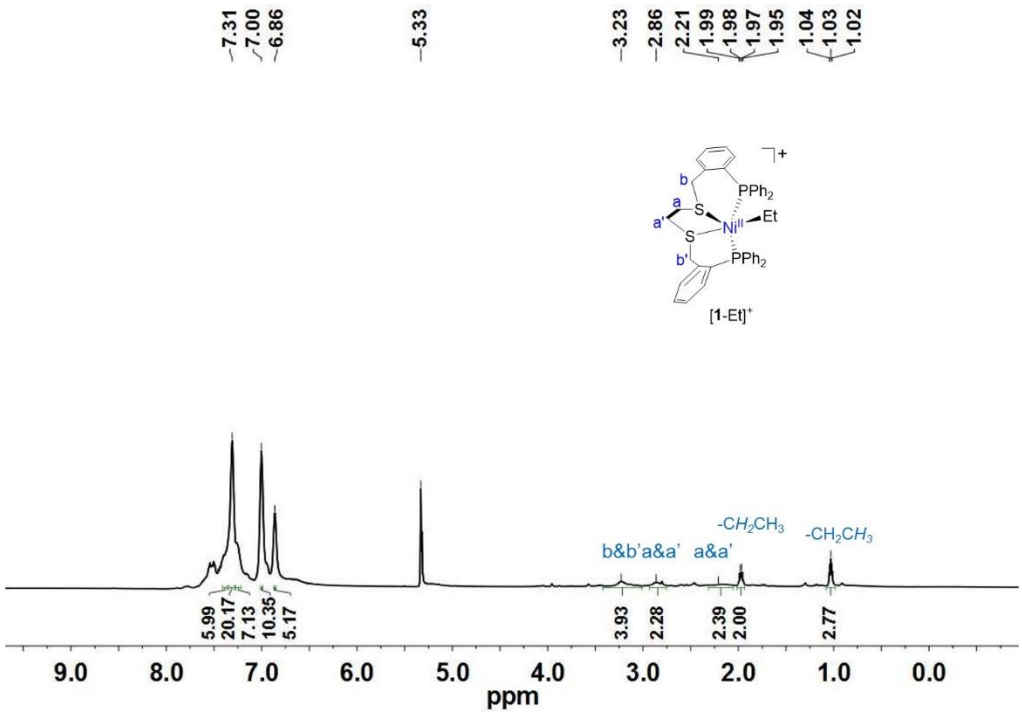

Fig. S13 ^{1}H NMR spectrum of [**1**−Et]BPh_4 in CD_2Cl_2.

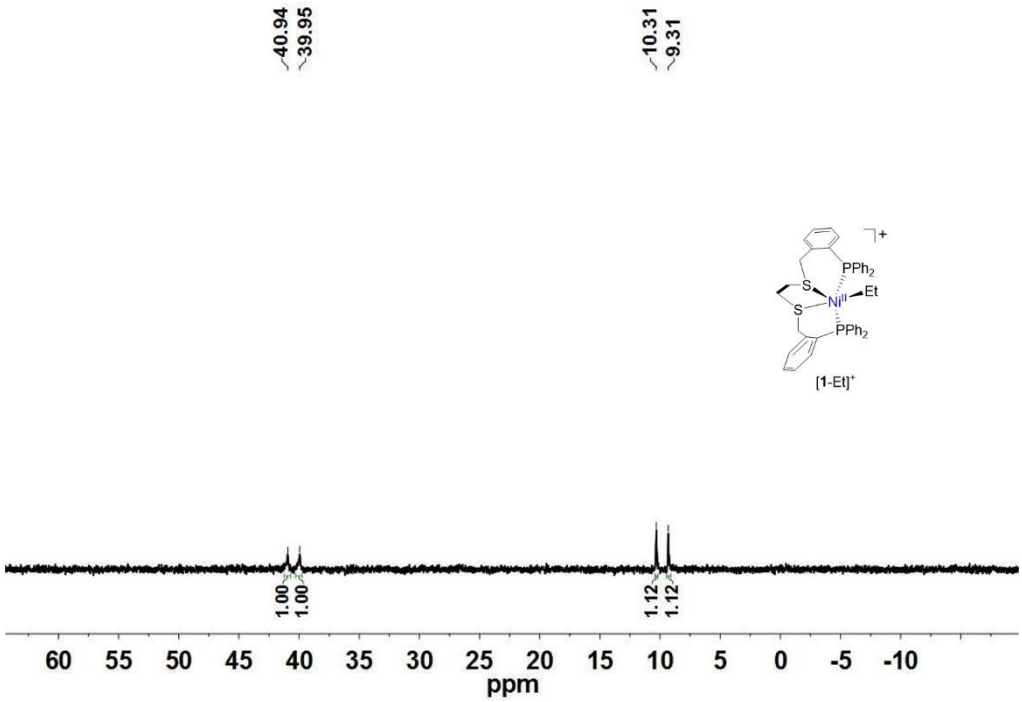

Fig. S14 ^{31}P NMR spectrum of [**1**−Et]BPh_4 in CD_2Cl_2.

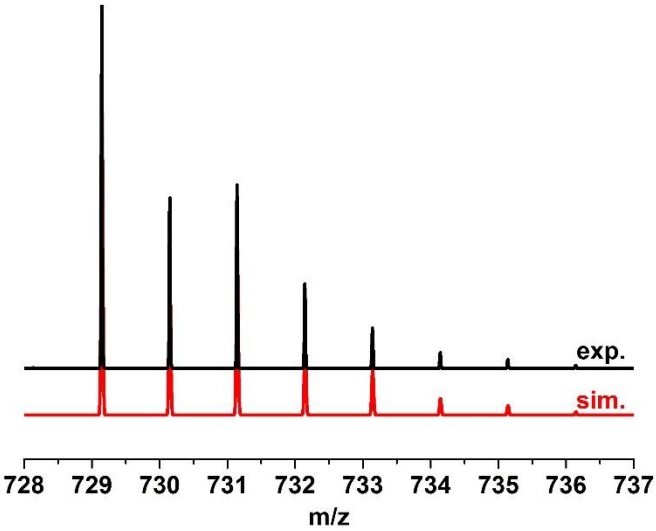

Fig. S15 ESI-MS spectrum of [**1**−Et]BPh_4 in CH_2Cl_2.

Results:

Calcd for [**1**−Et]BPh_4, 729.1478; found, 729.1457.

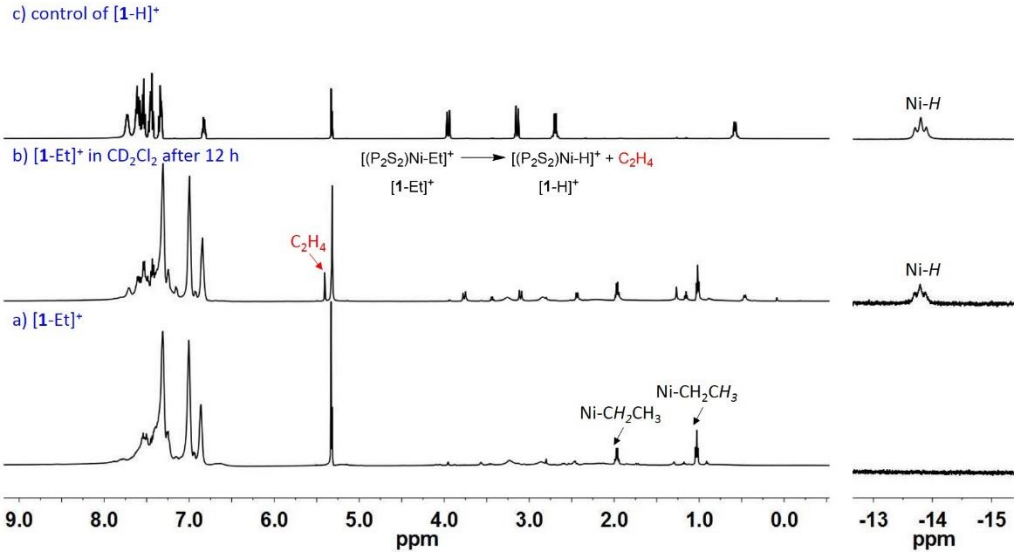

Fig. S16 ^{1}H NMR spectra of (a) [**1**-Et]$^+$. (b) [**1**-Et]$^+$ in CD_2Cl_2 after 12 h. (c) control of [**1**-H]$^+$.

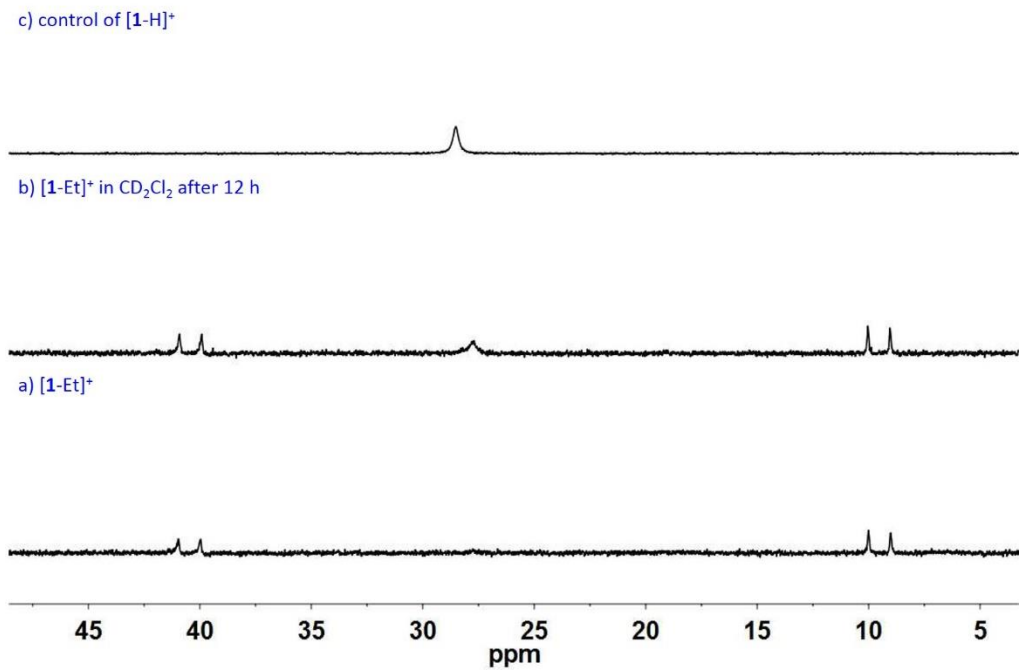

Fig. S17 ^{31}P NMR spectra of (a) [**1**-Et]$^{+}$. (b) [**1**-Et]$^{+}$ in CD_2Cl_2 after 12 h. (c) control of [**1**-H]$^{+}$.

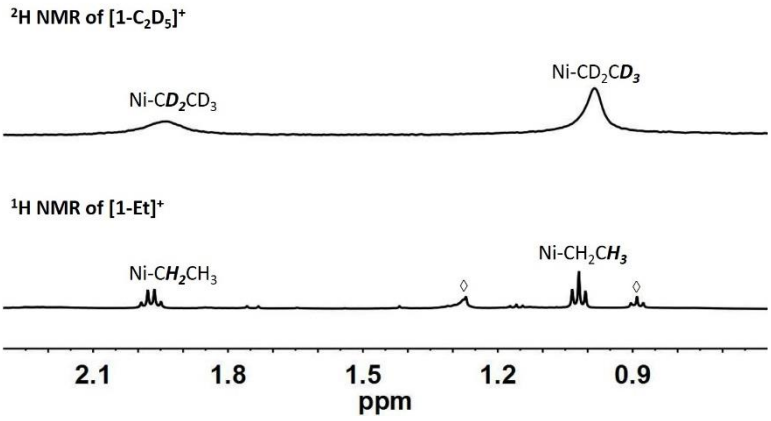

Fig. S18 ^{1}H NMR (CD_2Cl_2) spectrum of [**1**−Et]$^+$ and ^{2}H NMR (CH_2Cl_2) spectrum of [**1**−C_2D_5]$^+$, respectively. Assignments: (The peaks marked with ◊ is assigned to residual solvent protons of hexane.)

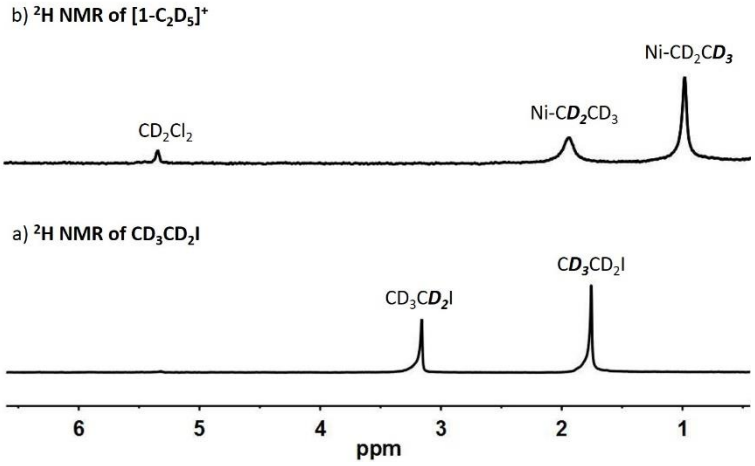

Fig. S19 a) ^{2}H NMR (CH_2Cl_2) spectrum of CD_3CD_2I. b) ^{2}H NMR (CH_2Cl_2) spectrum of [**1**-C_2D_5]BPh_4.

Results: a) δ 1.76 (br, C*D*$_3$CD$_2$I), 3.16 (br, CD$_3$C*D*$_2$I).

b) δ 0.99 (br, Ni−CD$_2$C*D*$_3$), 1.95 (br, Ni−C*D*$_2$CD$_3$).

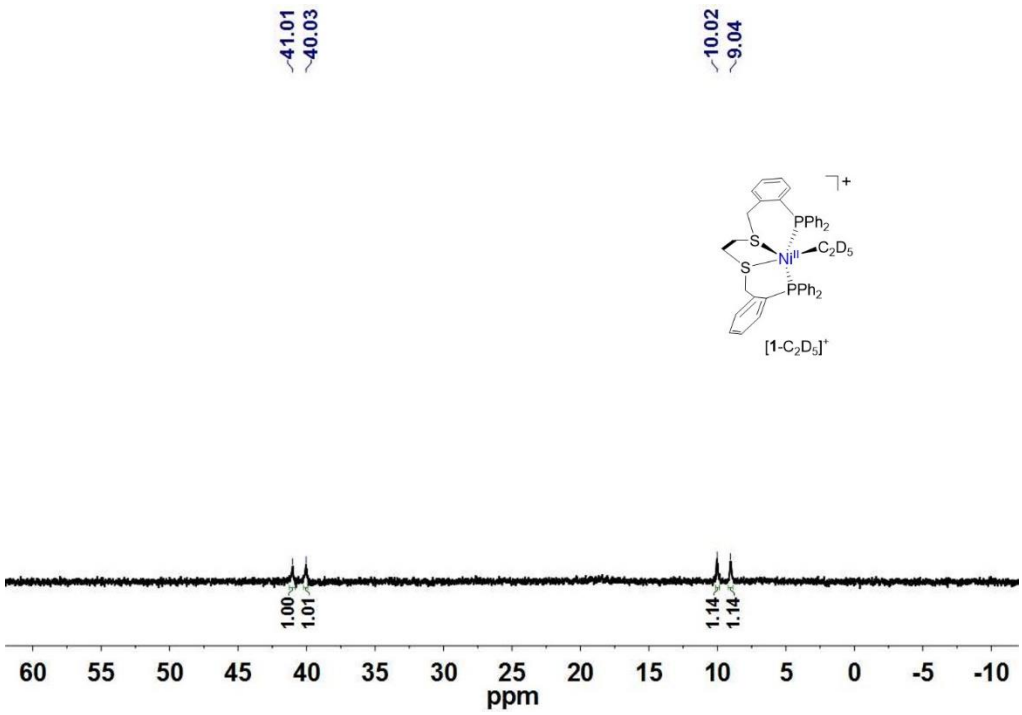

Fig. S20 ^{31}P NMR spectrum of [**1**−C_2D_5]BPh_4 in CH_2Cl_2.

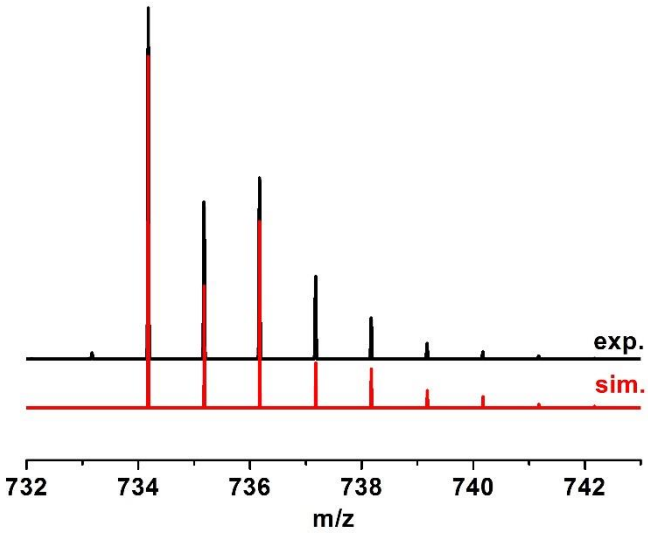

Fig. S21 ESI-MS spectrum of [**1**−C_2D_5]BPh_4 in CH_2Cl_2.

Results:

Calcd for [**1**−C_2D_5]BPh_4, 734.1792; found,734.1768.

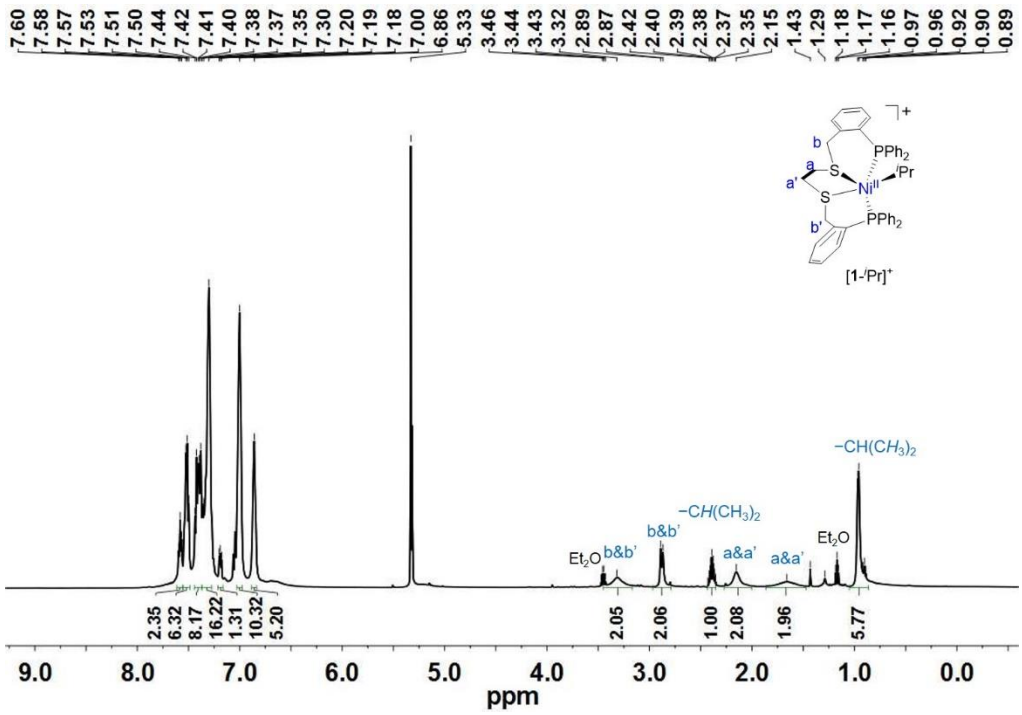

Fig. S22 ^{1}H NMR spectrum of [**1**–^{i}Pr]BPh_4 in CD_2Cl_2.

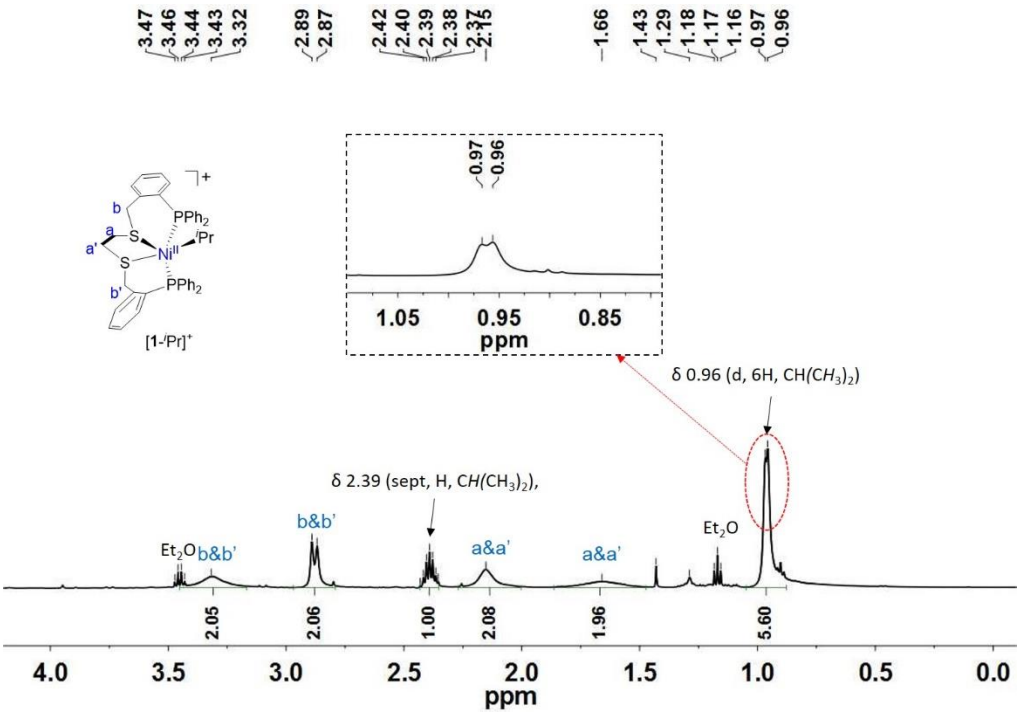

Fig. S23 ^{1}H NMR spectrum (500 MHz, CD_2Cl_2) of [**1**–^{i}Pr]$^+$: expansion of the δ 4.2-(-0.1) region.

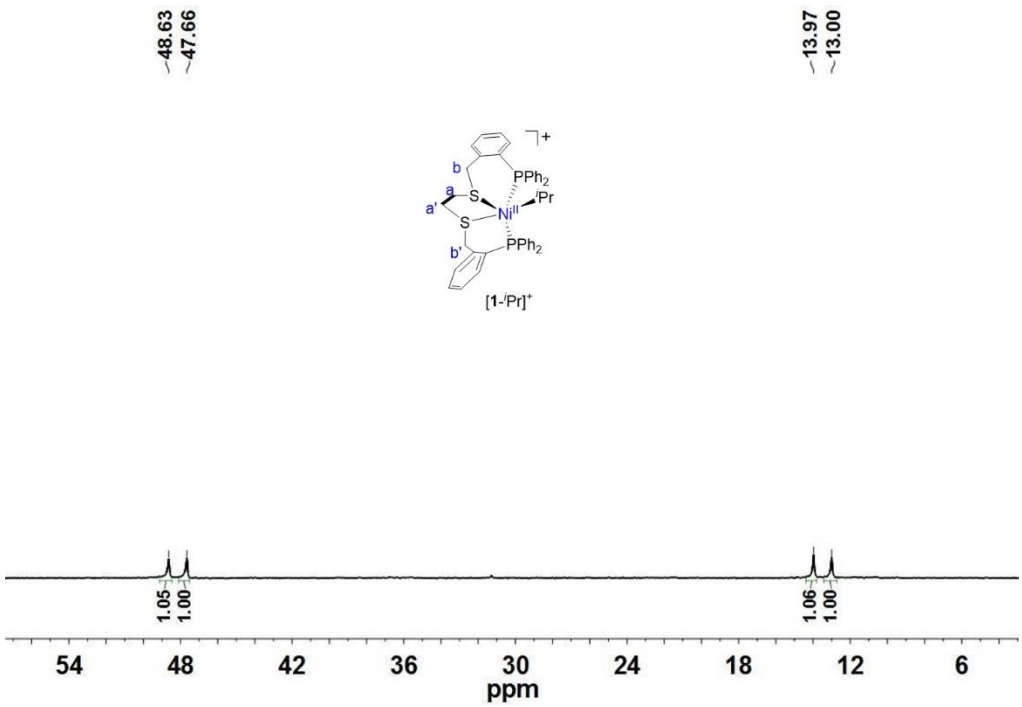

Fig. S24 ^{31}P NMR spectrum of [**1**−^{i}Pr]BPh_4 in CD_2Cl_2 at 213 K.

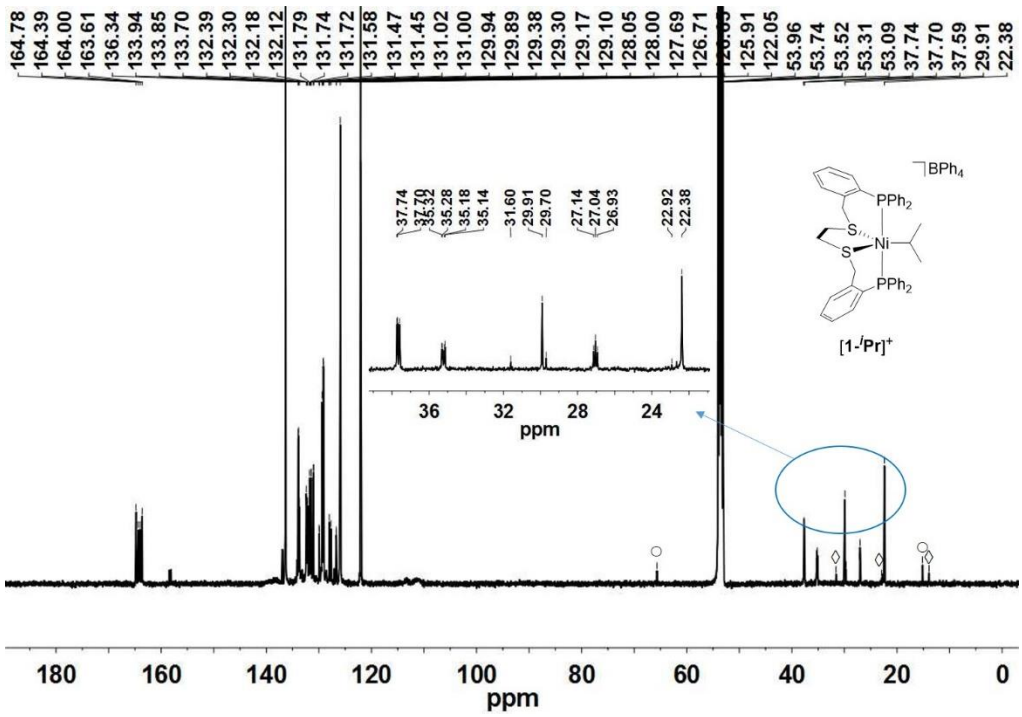

Fig. S25 ^{13}C NMR spectrum (126 MHz, CD_2Cl_2) of [**1**–^{i}Pr]BPh_4.

Assignments: (The peaks marked with ◊ and ○ are assigned to residual solvent protons of hexane and diethyl ether.)

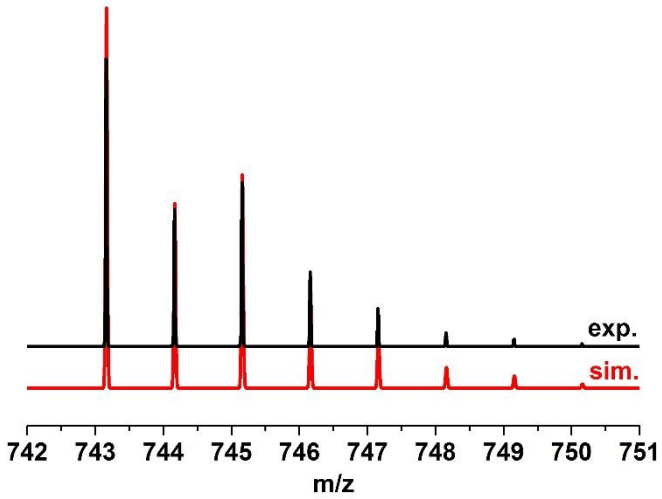

Fig. S26 ESI-MS spectrum of [**1**-^{i}Pr]BPh_4 in CH_2Cl_2.

Results:

Calcd for [**1**-^{i}Pr]BPh_4, 743.1635; found, 743.1600.

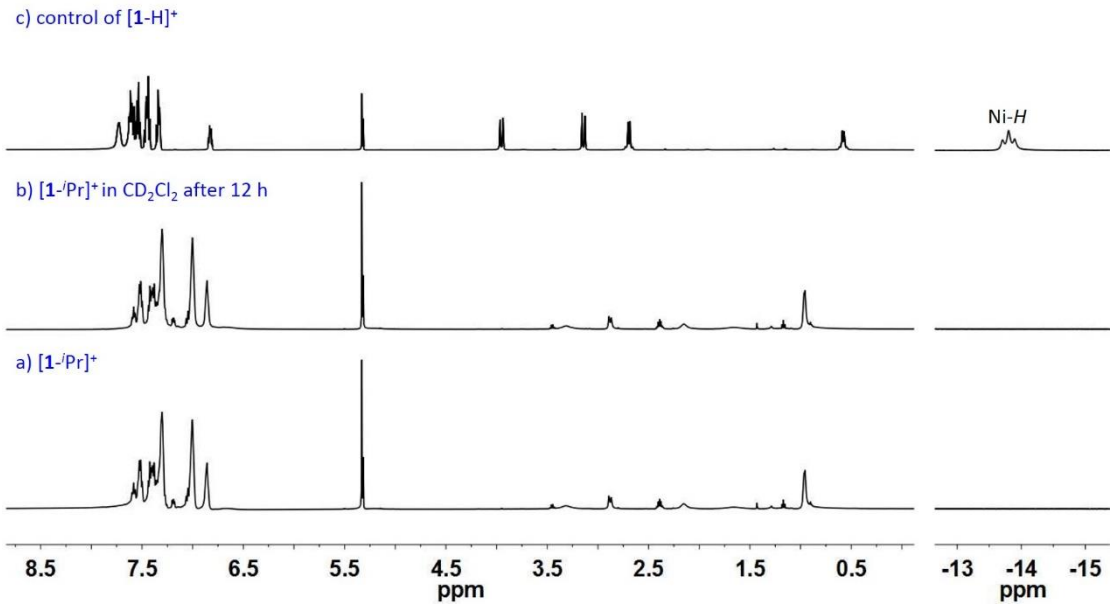

Fig. S27 ^{1}H NMR spectra in CD_2Cl_2 for (a) [**1**-^{i}Pr]$^+$. (b) [**1**-^{i}Pr]$^+$ in CD_2Cl_2 after 12 h. (c) control of [**1**-H]$^+$.

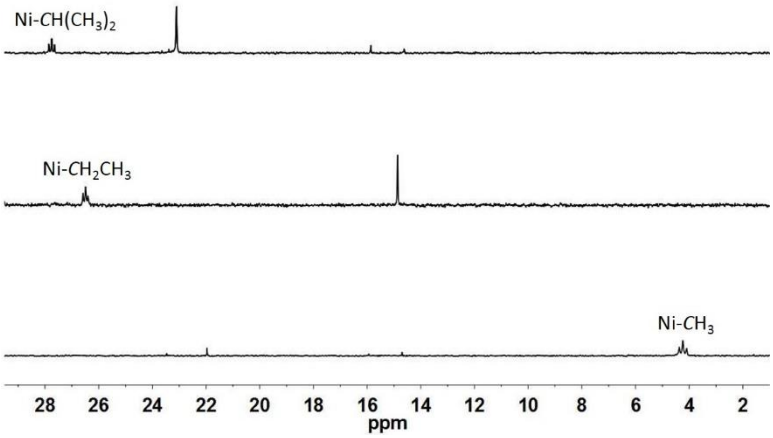

Fig. S28 ^{13}C NMR spectra of [**1**−CH_3]$^+$, [**1**−Et]$^+$ and [**1**−^{i}Pr]$^+$ (126 MHz, CD_2Cl_2): expansion of the δ 29.5 -1 region.

Results:

^{13}C NMR (126 MHz, CD_2Cl_2): δ 4.23 (t, $J_{P\text{-}C}$ = 17.1 Hz, Ni-*C*H_3)

δ 26.49 (t, $J_{P\text{-}C}$ = 11.7 Hz, Ni-*C*H_2CH_3)

δ 27.75 (t, $J_{P\text{-}C}$ = 13.2 Hz, Ni-*C*H(CH_3)$_2$)

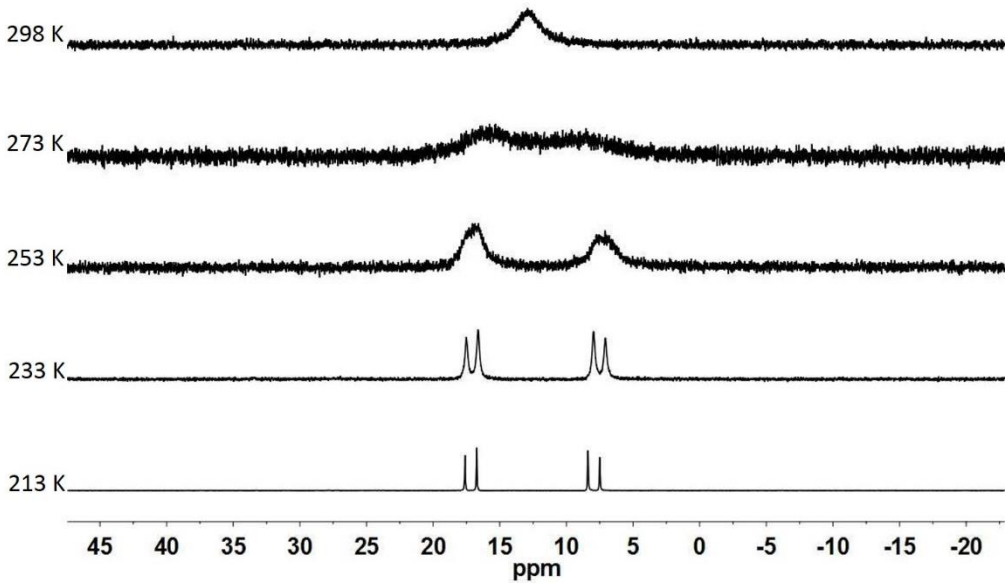

Fig. S29 VT ^{31}P NMR spectra (202 MHz, CD_2Cl_2) of [**1**−CH_3]BPh_4.

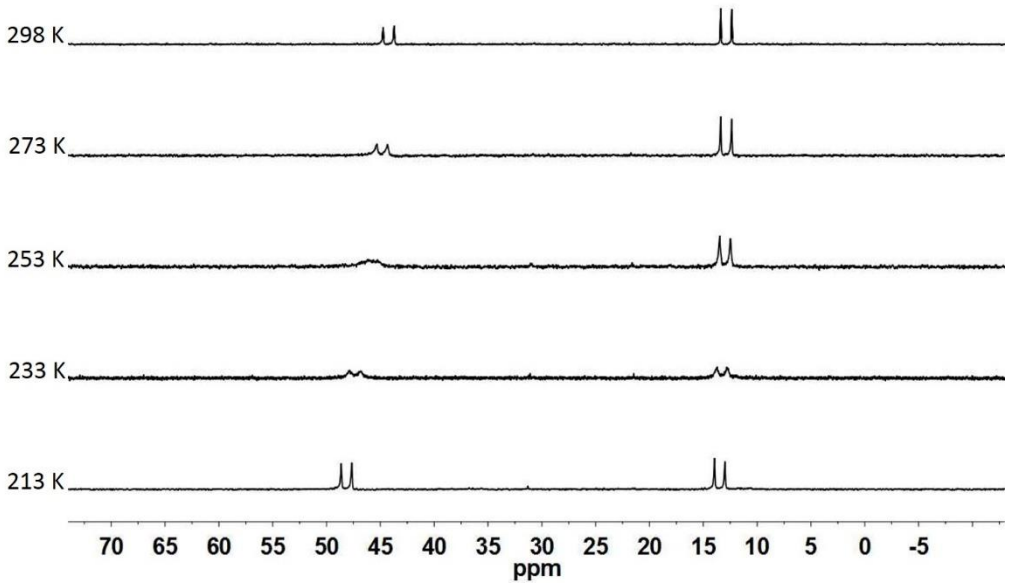

Fig. S30 VT ^{31}P NMR spectra (202 MHz, CD_2Cl_2) of [**1**–^{i}Pr]BPh_4.

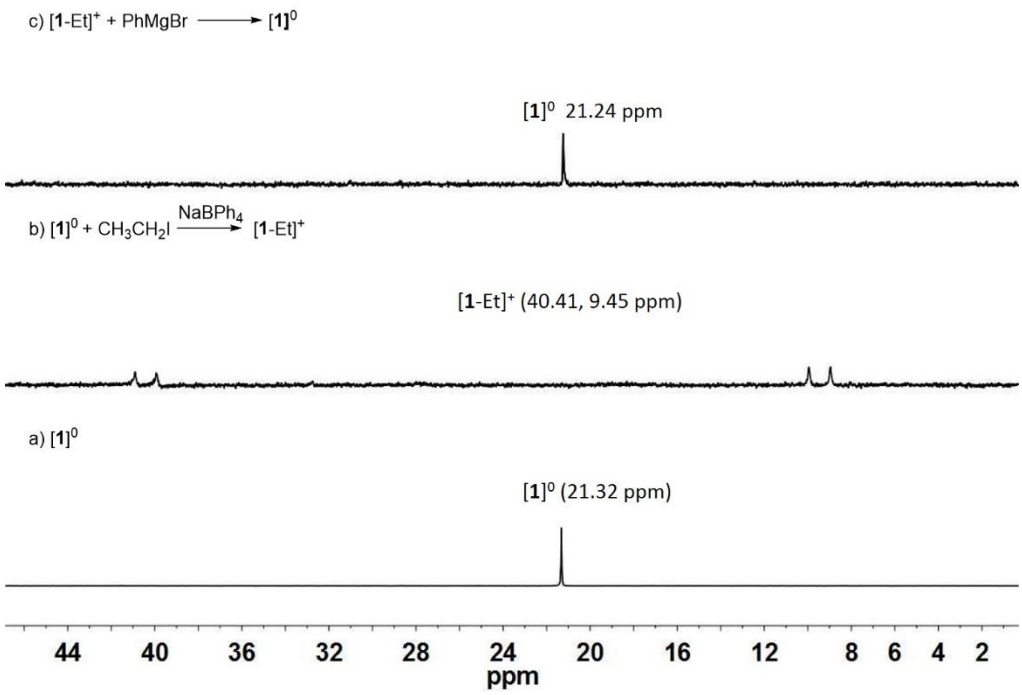

Fig. S31 ^{31}P NMR spectra for (a) [**1**]^0 in THF. (b) the reaction of [**1**]^0 with iodoethane, and then was treated with $NaBPh_4$, producing [**1**−Et]$^+$ in THF. (c) the reaction of [**1**−Et]$^+$ with PhMgBr, producing [**1**]^0 in THF.

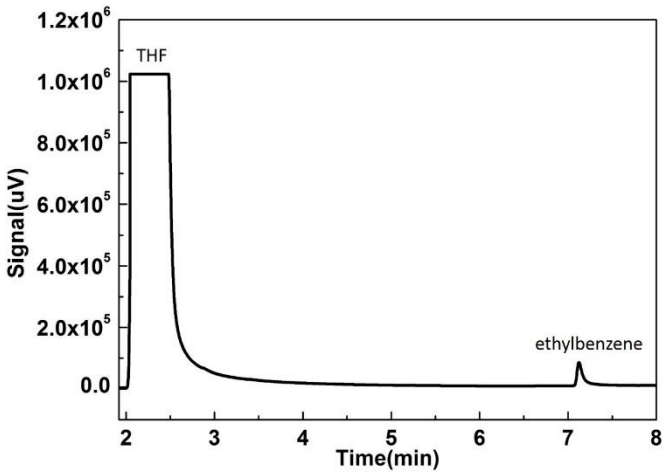

Fig. S32 GC-FID of ethylbenzene standard in THF.

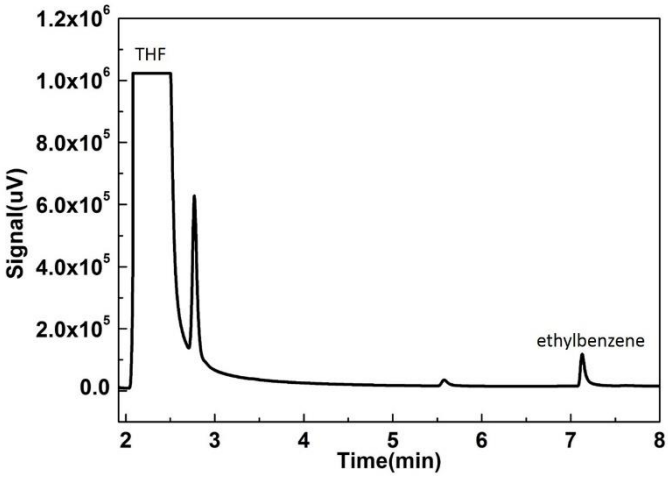

Fig. S33 GC-FID of the reaction mixture of [**1**−Et]$^+$ with PhMgBr in THF.

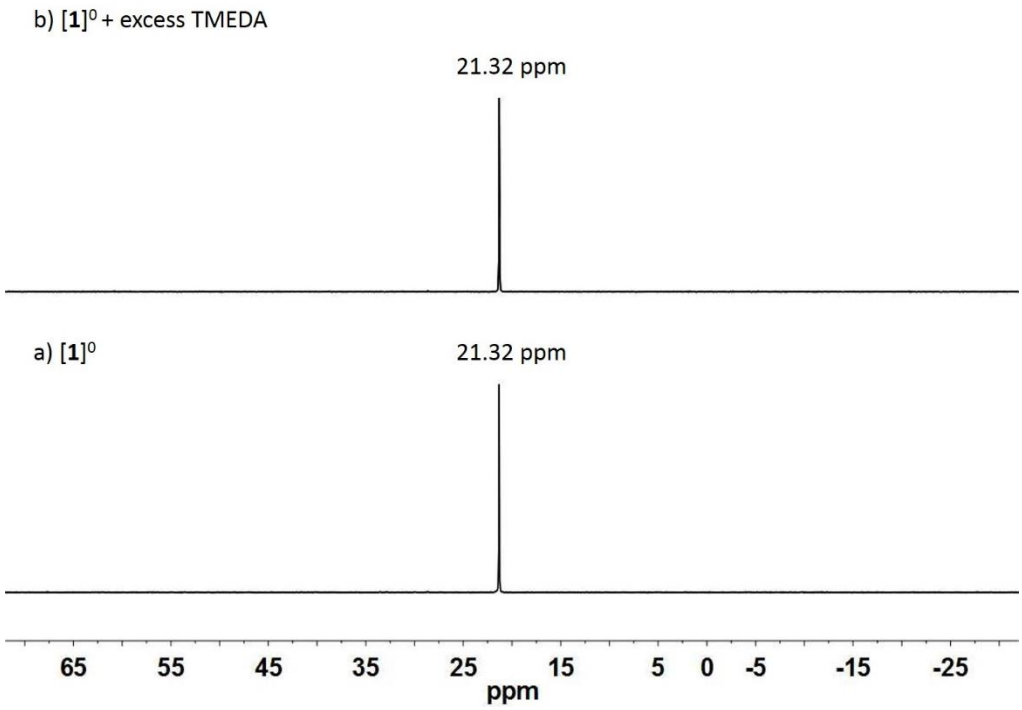

Fig. S34 $^{31}P\{^{1}H\}$ NMR spectra recorded for the reaction of [**1**]^{0} with tetramethylethylenediamine (TMEDA).

Results:

No reaction occurred as monitored by ^{31}P NMR spectroscopy.

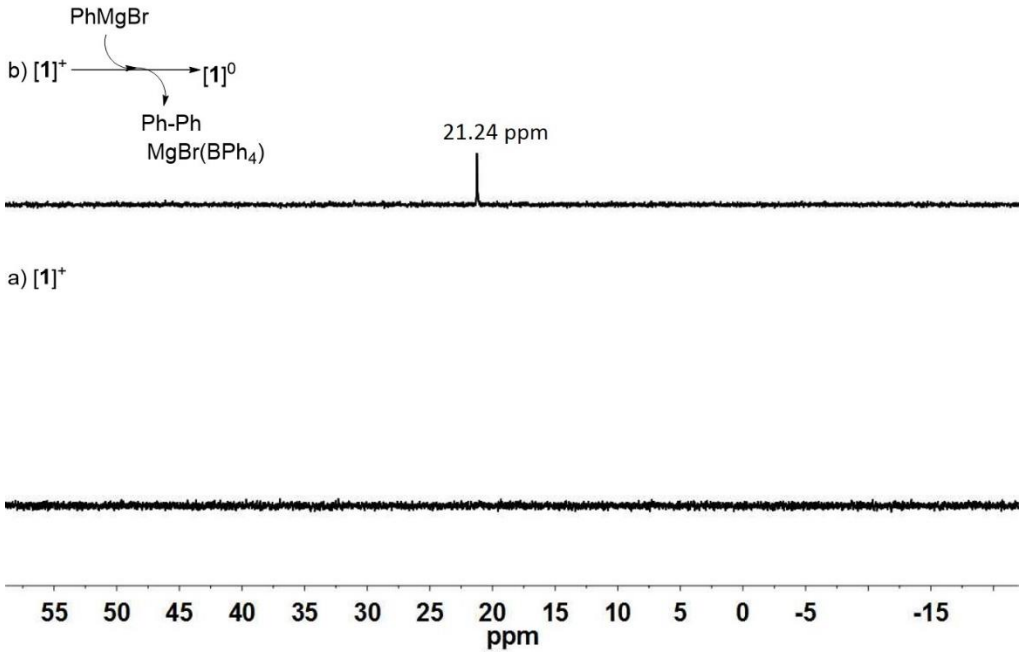

Fig. S35 $^{31}P\{^{1}H\}$ NMR spectra recorded for the reaction of [**1**]$^{+}$ with PhMgBr.

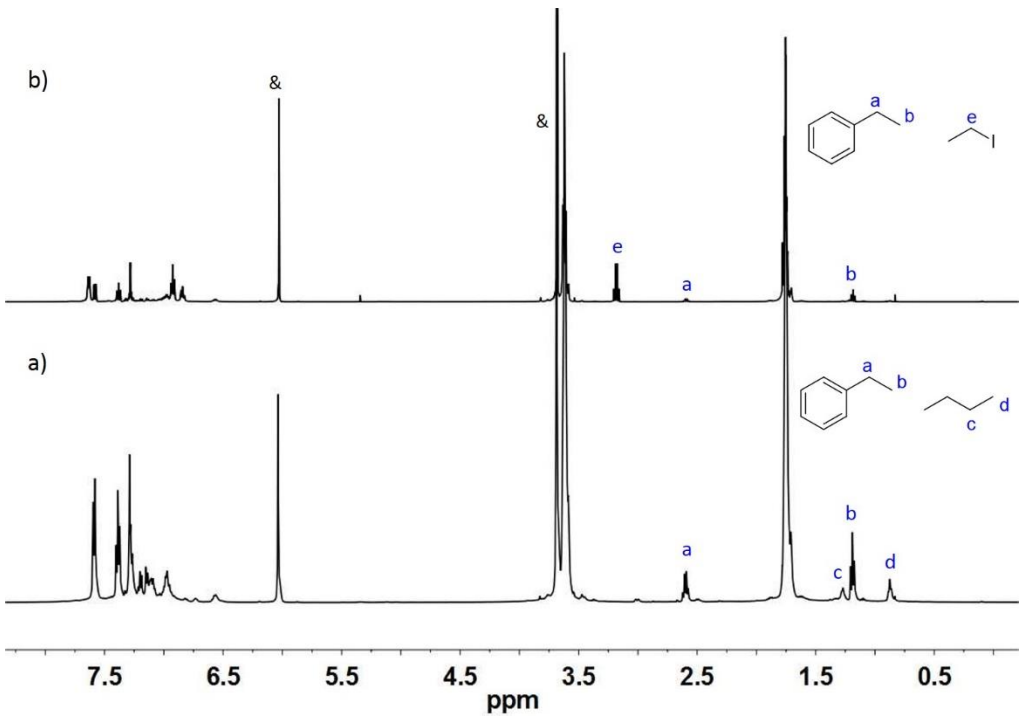

Fig. S36 ^{1}H NMR spectra for (a) the reaction of CH_3CH_2I and PhMgBr with the catalysis of [**1**]^0 in THF-d_8 for 15 min, (b) the control experiment for the reaction of CH_3CH_2I and PhMgBr in the absence of catalyst. 1,3,5-Trimethoxybenzene was added to this solution as an internal standard, & = 1,3,5-trimethoxybenzene.

Table S1 Coupling reactions of alkyl halides with Grignard reagents catalyzed by [**1**]^0.

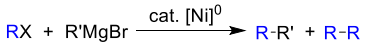

Entry	Alkyl halide	Grignard Reagent	Product Yield(%)[a,b]	
			R-R'	R-R
1	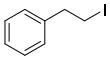	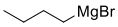	74	12
2	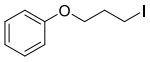	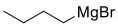	67	15
3	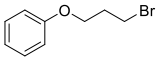	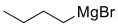	42	25
4	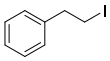		51[c]	trace
5	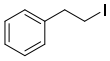	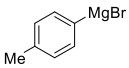	77	11
6			55	–[d]
7		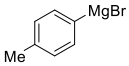	62	–[d]

[a]All reactions were carried out by adding the aryl Grignard reagent (0.5 mmol) dropwise to a mixture of the alkyl halide (0.5 mmol), $Ni^0(P_2S_2)$ (2 mol %), TMEDA (30 mol %) in 1 mL THF at 0°C for 2 h , the conversion of alkyl halide was 100%. [b]Yield was determined by ^{1}H-NMR spectroscopy (1,3,5-trimethoxybenzene as the internal standard). [c]Reaction conducted at 25°C and the conversion of alkyl halide was 56%.[d]Yield was unable to be determined by ^{1}H NMR spectroscopy due to the significant overlap between the byproduct peaks and the solvent peaks.

Single-crystal X-ray diffraction data of $[\mathbf{1}]^0$, $[\mathbf{1}]^+$, $[\mathbf{1}-\text{allyl}]^+$ were collected on a Rigaku Oxford Diffraction XtaLAB Synergy diffractometer equipped with a HyPix-6000HE area detector at 100 K using Mo Kα (λ = 0.71073 Å) from PhotonJet micro-focus X-ray Source. The structure was solved using the charge-flipping algorithm, as implemented in the program *SUPERFLIP*[1] and refined by full-matrix least-squares techniques against *Fo*[1] using the SHELXL program[2] through the OLEX2 interface.[3]

Table S2 Crystal data and structure refinement parameters for $[\mathbf{1}]^0$.

Empirical formula	$C_{44}H_{44}NiOP_2S_2$
Formula weight	773.56
Crystal system	triclinic
Space group	*P*-1
Unit cell dimensions	a = 9.5713(3) Å
	b = 13.7242(5) Å
	c = 14.7211(3) Å
	α = 85.898(2) °
	β = 86.077(2) °
	γ = 80.810(3) °
Volume	1900.83(9) $Å^3$
Z	2
Density (calculated)	1.352 g/cm^3
Absorption coefficient	2.814 mm^{-1}
F(000)	812.0
Theta range for data collection	8.62 to 134.144
Index ranges	$-11 \leq h \leq 11$,
	$-16 \leq k \leq 16$,
	$-10 \leq l \leq 17$
Reflections collected	17621
Independent reflections	6728 [R_{int} = 0.0358, R_{sigma} = 0.0410]
Absorption correction	multi-scan
Refinement method	Full-matrix least-squares on F^2
Data / restraints / parameters	6728/0/469
Goodness-of-fit on F^2	1.067
Final R indices [I>2sigma(I)]	R_1 = 0.0344, wR_2 = 0.0841
R indices (all data)	R_1 = 0.0459, wR_2 = 0.0908
Largest diff. peak and hole	0.62 and -0.42 e.$Å^{-3}$

Table S3 Crystal data and structure refinement parameters for [**1**]BPh_4.

Empirical formula	$C_{64}H_{56}BNiP_2S_2$
Formula weight	1020.66
Crystal system	orthorhombic
Space group	*Pbca*
Unit cell dimensions	a = 18.6906(3) Å
	b = 21.6675(3) Å
	c = 27.8121(4) Å
	α =90 °
	β =90 °
	γ =90 °
Volume	11263.4(3) $Å^3$
Z	8
Density (calculated)	1.204 g/cm^3
Absorption coefficient	2.009 mm^{-1}
F(000)	4280.0
Theta range for data collection	7.008 to 134.16 °
Index ranges	$-22 \leq h \leq 22$,
	$-14 \leq k \leq 25$,
	$-32 \leq l \leq 33$
Reflections collected	34031
Independent reflections	9960 [R_{int} = 0.0433, R_{sigma} = 0.0428]
Absorption correction	multi-scan
Refinement method	Full-matrix least-squares on F^2
Data / restraints / parameters	9960/0/631
Goodness-of-fit on F^2	1.027
Final R indices [I>2sigma(I)]	R_1 = 0.0391, wR_2 = 0.0987
R indices (all data)	R_1 =0.0513, wR_2 = 0.1088
Largest diff. peak and hole	0.31 and -0.30 e.$Å^{-3}$

Table S4 Crystal data and structure refinement parameters for [**1**−allyl]BPh_4.

Empirical formula	$C_{67}H_{61}BNiP_2S_2$
Formula weight	1061.73
Crystal system	triclinic
Space group	*P*-1
Unit cell dimensions	a = 11.4951(1) Å
	b = 13.9481(1) Å
	c = 17.4387(1) Å
	α = 91.9485(8) °
	β = 103.1258(10) °
	γ = 97.6660(9) °
Volume	2692.67(5) $Å^3$
Z	2
Density (calculated)	1.310 g/cm^3
Absorption coefficient	2.122 mm^{-1}
F(000)	1116.0
Theta range for data collection	7.982 to 154.278 °
Index ranges	$-14 \leq h \leq 12$,
	$-17 \leq k \leq 17$,
	$-19 \leq l \leq 21$
Reflections collected	28724
Independent reflections	10630 [R_{int} = 0.0495, R_{sigma} = 0.0502]
Absorption correction	multi-scan
Refinement method	Full-matrix least-squares on F^2
Data / restraints / parameters	10630/0/667
Goodness-of-fit on F^2	1.066
Final R indices [I>2sigma(I)]	R_1 = 0.0494, wR_2 = 0.1320
R indices (all data)	R_1 = 0.0604, wR_2 = 0.1462
Largest diff. peak and hole	0.65 and -0.60 e.$Å^{-3}$

RERFERENCES

1 L. Palatinus and G. Chapuis, Superflip- a computer program for the solution of crystal structures by charge flipping in arbitrary dimensions. *J Appl Crystallogr,* 2007, **40**, 786–790.

2 G. M. Sheldrick, Crystal structure refinement with Shelxl. *Acta Cryst. C,* 2015, **71**, 3–8.

3 O. V. Dolomanov, L. J. Bourhis, R. J. Gildea, J. A. K. Howard and H. Puschmann, Olex2: a complete structure solution, refinement and analysis program. *J Appl Crystallogr,* 2009, **42**, 339–341.